


Article

Direct Synthesis of Dimethyl Ether from CO₂ Hydrogenation over Core-Shell Nanotube Bi-Functional Catalyst

Mohamed Yusuf Mohamud ^{1,2}, Tuan Amran Tuan Abdullah ^{1,2,*}, Arshad Ahmad ^{1,2}, Muhammad Ikram ^{3,*}, Afizah Alir ^{1,2}, Melissa Low Phey Phey ^{1,2} and Walid Nabgan ^{4,*}

¹ Faculty of Chemical and Energy Engineering, Universiti Teknologi Malaysia, Johor Bahru 81310, Malaysia

² Centre of Hydrogen Energy, Institute of Future Energy, Johor Bahru 81310, Malaysia

³ Solar Cell Applications Research Lab, Department of Physics, Government College University Lahore, Punjab 54000, Pakistan

⁴ Departament d'Enginyeria Química, Universitat Rovira I Virgili, Av Països Catalans 26, 43007 Tarragona, Spain

* Correspondence: tuanamran@utm.my (T.A.T.A.); dr.muhammadikram@gcu.edu.pk (M.I.); walid.nabgan@urv.cat (W.N.)

Abstract: Directly synthesising dimethyl ether (DME) from CO₂ hydrogenation is a promising technique for efficiently utilising CO₂ as a feedstock to produce clean fuel. The main challenges in this process are the low CO₂ conversion and DME selectivity of the catalyst and its deactivation over time due to sintering, aggregation, coke formation, and water adsorption. This study aimed to develop a dual-functional, halloysite nanotube-supported CuZnO-PTA catalyst with a core-shell structure and investigate the effects of the active site mass ratio CuZnO/PTA on CO₂ conversion and DME selectivity. A dual-functional core-shell mesopores halloysite nanotube (HNT) catalyst was developed, and both active sites were co-hosted on one support. The co-impregnation method was used to synthesise CuZnO and 12-phosphotungstic acids (PTA) that were then supported by a mesoporous core-shell (HNT). BET surface area, N₂ physisorption, FE-SEM, SEM, XRD, H₂-TPR, and NH₃-TPD of the core-shell catalyst characterised physio-chemical properties of the prepared hybrid catalyst. The experimental results showed that the synthesised CuZn-PTA@HNT core-shell bifunctional catalyst was promising; the CO₂ conversion was almost the same for all four catalysts, with an average of 22.17%, while the DME selectivity reached 68.9%. Furthermore, the effect of both active sites on the hybrid catalyst was studied, and the metal Cu wt% mass ratio loading was not significant. In contrast, the PTA acid sites positively affected DME selectivity; they also showed an excellent tolerance towards the water generated in the methanol dehydration reaction. In addition, the effect of the temperature and reusability of the CZ-PTA@HNT catalyst has also been investigated, and the results show that increasing the temperature improves CO₂ conversion but decreases DME selectivity. A temperature of less than 305 °C is a good compromise between CO₂ conversion and DME selectivity, and the catalyst also showed good stability and continuous activity/stability over five consecutive cycles. In conclusion, this study presents a novel approach of using a core-shell halloysite nanotube-supported CuZnO-PTA catalyst to directly synthesise dimethyl ether (DME) from CO₂ hydrogenation which exhibits promising results in terms of CO₂ conversion and DME selectivity.

Keywords: CO₂ hydrogenation; dimethyl ether; core-shell nanotube; Cu/ZnO; phosphotungstic acid; halloysite nanotube



Citation: Mohamud, M.Y.; Abdullah, T.A.T.; Ahmad, A.; Ikram, M.; Alir, A.; Phey, M.L.P.; Nabgan, W. Direct Synthesis of Dimethyl Ether from CO₂ Hydrogenation over Core-Shell Nanotube Bi-Functional Catalyst. *Catalysts* **2023**, *13*, 408. <https://doi.org/10.3390/catal13020408>

Academic Editors: Sebastiano Campisi, Ridha Djellabi and Melissa Greta Galloni

Received: 12 January 2023

Revised: 12 February 2023

Accepted: 13 February 2023

Published: 14 February 2023



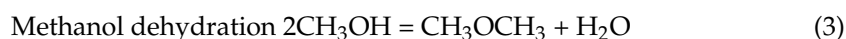
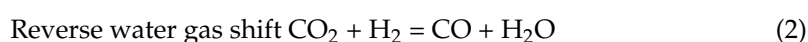
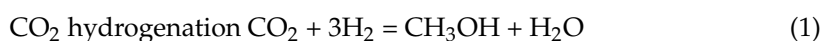
Copyright: © 2023 by the authors. Licensee MDPI, Basel, Switzerland. This article is an open access article distributed under the terms and conditions of the Creative Commons Attribution (CC BY) license (<https://creativecommons.org/licenses/by/4.0/>).

1. Introduction

Global warming is one of the most significant environmental phenomena attributed to human activity-related CO₂ emissions [1,2]. Unfortunately, burning carbon-based fossil fuels releases a lot of CO₂, which disrupts the earth's natural carbon cycle and causes global warming, acidification of the oceans, rising sea levels, and climate change [3]. Therefore, converting CO₂ into value-added chemicals such as CO, methanol, dimethyl ether, methane,

formic acid, urea, and other hydrocarbons is feasible to mitigate CO₂ emissions [4,5]. In this study, dimethyl ether was found to be a highly efficient alternative fuel for use in diesel engines, primarily due to its high oxygen concentration of approximately 35% by mass, its molecular structure without C–C bonds, low ignition temperature, and its ability to rapidly vaporize when introduced into the cylinder. This leads to almost smoke-free combustion [6,7].

Traditionally, the production of dimethyl ether (DME) has been achieved through a two-step process, starting with the synthesis of methanol (MeOH) from syngas over a Cu-based Cu/ZnO/Al₂O₃ (CZA) catalyst and ending with the dehydration of MeOH to DME on a solid acid catalyst, such as γ -alumina [8] or zeolites, particularly ZSM-5 [9]. In addition, to reverse water gas shift reaction as an intermediate [10]. DME has been synthesised directly from CO₂ hydrogenation based on the following three sets of reactions:



From a catalytic perspective, the literature has paid remarkable attention to developing suitable hybrid catalysts for directly synthesising DME from CO₂ hydrogenation [11]. Copper-based catalysts have been one of the nonprecious metals used in CO₂ hydrogenation, which received the most significant research attention [12]; besides its abundance and low cost, Cu exhibits high activity and selectivity towards methanol [13]. The most widely used catalyst system in the synthesis of DME from CO₂ hydrogenation is a mixture of methanol synthesis and methanol dehydration catalysts, particularly the CuZnAl catalyst combined with ZSM-5 or γ -Al₂O₃ [14]. However, the low conversion in CO₂ hydrogenation can be attributed to several significant factors, including the thermodynamic inertness of CO₂, the generation of water as a by-product, the formation of coke, sintering, and the accumulation of Cu particles, which is considered a critical factor in catalyst deactivation [15]. During the direct synthesis of dimethyl ether (DME) from carbon dioxide (CO₂) hydrogenation, water is produced as an intermediate product through two main reactions: the reverse water gas shift reaction (RWGS) and methanol dehydration. One significant challenge in this process is the tendency of H₂O molecules from RWGS to strongly adsorb on copper (Cu) particles, causing aggregation and early deactivation of the catalyst [16]. In addition, producing water molecules as a by-product during the methanol dehydration step can also create challenges. The competition between water and synthesised DME for binding to the active sites of the catalyst acid can also reduce DME selectivity and lead to the deactivation of the acid sites. These factors can all contribute to the low conversion and selectivity of the catalyst in synthesising DME from CO₂ hydrogenation [17].

Developing an active and stable bifunctional hybrid catalyst for a reaction that involves both hydrogenation and dehydration is challenging due to the difficulties as mentioned earlier. Various strategies have been proposed and investigated to reduce or eliminate the catalyst activity and stability drawbacks, including the replacement of the active metals [18], essential features of promoters [19], interactions between active metals and support [3], particle size reduction [20], pre-treatment and preparation method changes [21,22], and viability testing for different combinations of metals and supports [16]. Therefore, developing a hybrid catalyst with an excellent contact state between the methanol synthesis catalyst and dehydration catalyst is vital [23]. Using catalyst particles with a core-shell structure is a promising approach for preserving metallic properties while reducing their sintering, aggregation, and coke formation due to side reactions [24]. In addition, separating individual reactions into different catalyst particle regions enhances the catalytic particle's selectivity in such a series of complex reactions [12].

A significant amount of research has focused on developing core-shell supports for CuZnO metal nanoparticles using materials such as silica, alumina, zeolites, and Silica-Alumina-Phosphate (SAPO) mesoporous materials. These core-shell structures can poten-

tially improve the stability and activity of CuZnO catalysts and prevent the aggregation of CuZnO nanoparticles [25]. Recently, Karaman et al. demonstrated the effectiveness of a mesoporous alumina-encapsulated Cu-ZnO-Al (CZA) catalyst with a core-shell structure synthesized through the hydrothermal method in the conversion of syngas and CO₂ to dimethyl ether [26]. The core-shell system has also been found to provide excellent resistance to the sintering of Cu species in the core and to minimize the adverse effects of interaction between individual functions, which can lead to deactivation [27]. Furthermore, Yang et al. [28] synthesized a core-shell catalyst with Cu and Cu/ZnO nanoparticles coated by mesoporous silica shells for CO₂ hydrogenation to methanol, demonstrating that the silica shell could effectively immobilize copper species and suppress the sintering of Cu nanoparticles during the reaction.

On the other hand, the core-shell structure of a catalyst particle is superior to a conventional physical admixture of individual functions in terms of activity and stability in the indirect synthesis of DME. Sánchez-Contador et al. [29] found that the core-shell catalyst, CZZr@S-11, prepared under appropriate conditions, demonstrated a better performance in the direct synthesis of DME from the joint hydrogenation of CO and CO₂ compared to the bifunctional catalyst (CZZr/S-11), which was created through a physical mixture of the individual components. The improved performance was attributed to the advantages of the core-shell structure. Cui, Xiaojing, et al. [30] encapsulated a commercial Cu/ZnO/Al₂O₃ catalyst onto a mesoporous SiO₂-Al₂O₃ core-shell, prepared through a hydrothermal method for the one-step synthesis of DME from CO₂ hydrogenation. The resulting CZAS@SA core-shell catalyst significantly improved the selectivity of DME and methanol, from 9.1 to 63.3 mol%.

Halloysite nanotube (HNT) is a natural clay mineral with a hollow nanotubular and unique scrolled structures consisting of kaolinite with a length of 0.4–1.5 μm, an outer diameter of 50–90 nm, and an inner lumen of 10–30 nm [31]. HNTs possess a positively-charged inner surface, which can interact with negatively-charged or electron-rich molecules. In contrast, the external surface, being negatively charged, can successfully bind with positively charged molecules [32]. Practically, (HNTs) possess several advantages, including high stability, resistance against organic solvents, ease of disposal or reusability, and availability in tons at low cost [33]. Furthermore, recent studies demonstrate the potential of halloysite clay nanotubes as catalyst support. Its good dispersibility of functionalized halloysite makes it an efficient surface-active catalyst. In addition, functionalized halloysite constitutes valuable support for metal nanoparticles, promoting catalytic applications with tuneable properties [34]. These characteristics make HNTs excellent vehicles for carrying numerous active sites when negatively charged molecules are sacked into the tube's lumen, and positive ones are adsorbed on the tube's outer surface [31].

Furthermore, the HNT outer surface charge can be improved by functionalization. The lumen can be modified or enlarged by selective alumina etching by intercalating its interlayer spacing [35]. Different molecules have been utilized, including amines [36]. Recently, Mazurova et al. and his team have proposed using HNTs as support for RuCo catalysts in Fischer-Tropsch synthesis. They found that HNTs loaded with bimetallic RuCo nanoparticles of 5–6 nm were more selective and active than systems based on synthetic aluminosilicates, silicates, and γ-Al₂O₃ [37]. Halloysite nanotubes can also be loaded with negatively-charged active species, which can be protected inside the inner lumen of the nanotubes. Lisuzzo et al. have successful loading of salicylic acid into the nanotubes was confirmed by Fourier-transform infrared (FTIR) spectroscopy, which evidenced the presence of the characteristic signals of the drug in the halloysite nanotubes (HNTs)/Salicylic acid (SA) hybrids [38]. This distinct feature of the charge state in HNT led us to the potential of electrostatically loading PTA anionic particles into the HNT's positively-charged lumen. Furthermore, the active metal (Cu) cations may also be deposited on the negatively-charged surface of the NHT. Therefore, we modified the HNT with DMF to increase the basal spacing and the lumen size, which may increase the loading of the bi-functional catalyst's methanol dehydration site (PTA) and enhance the surface absorption of the active metal (Cu).

This study aimed to develop a core-shell structure halloysite nanotube-supported CuZn-PTA@HNT catalyst. This catalyst aims to stabilize the CuZn metal site responsible for methanol synthesis on the outer negatively charged surface of the halloysite nanotubes (HNTs) and to load the PTA acid site responsible for methanol dehydration in the positively charged lumen of the HNTs. We also sought to investigate the effects of the active sites mass ratio CuZn/PTA on CO₂ conversion and DME selectivity. In addition, the influence of acid strength and water tolerance of the catalyst during the methanol dehydration reaction will be studied to understand how it affects the efficiency and stability of the reaction. Finally, the effect of temperature variation and stability of the most promising catalyst over five reaction cycles could be demonstrated, providing essential insights into the long-term performance of the catalyst.

2. Results and Discussion

HNTs have been proposed as a support for CuZn-PTA catalysts due to their unique porous structure and ability to host multiple active sites. Typically, HNTs have a hollow tubular structure consisting of an external surface with a negative charge. Moreover, a positively charged internal lumen has been confirmed through zeta-potential measurements. [32]. The XRD patterns in (Figure 1a) for both HNT and DMF-HNT showed similar peaks at 2θ 210.2, 11.8, 19.8, 24.8, 26.5, 34.8, 35.7, 38.1, 54.5, 62.3, 73.5, 77.13.

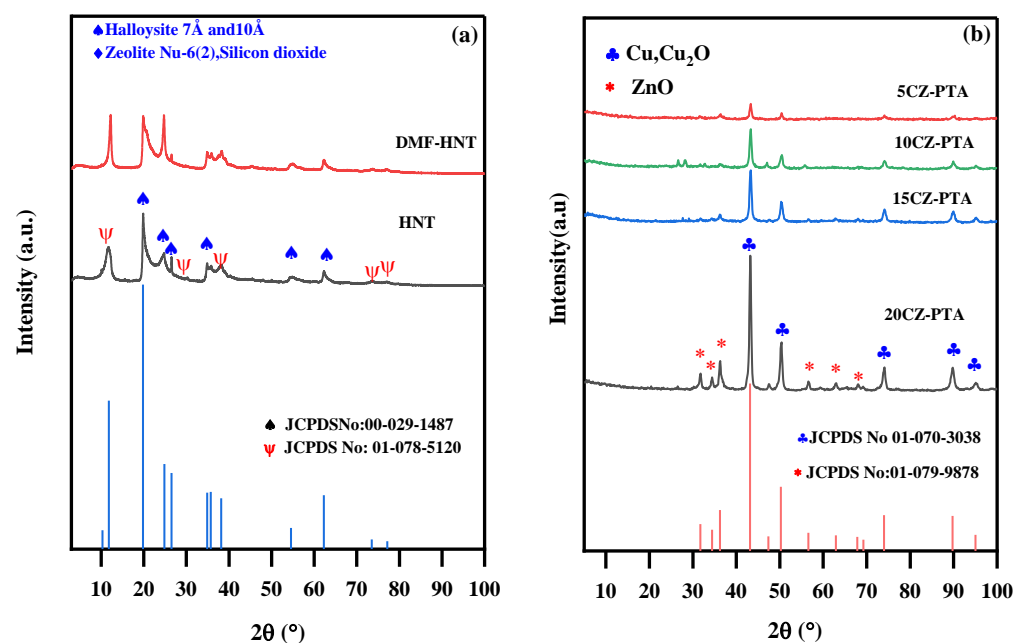


Figure 1. XRD pattern of the (a) HNT, modified-HNT, and (b) reduced CZ-PTA@HNT catalysts.

The peak positions are consistent with metallic Cu, Cu₂O, and ZnO at all potential peaks, indicating that the catalyst had a polycrystalline structure. Bragg's reflections for copper particles can be seen in the XRD pattern at 2θ values of 43.2, 47.3, 50.2, 56.5, 73.9, 89.7, 95.03, and 31.7, 34.4, 36.2, 67.8, 69.2, 62.8, respectively, representing different angles as (Figure 1b) illustrates [39,40]. Based on Scherrer's equation, the active metal Cu average particle crystallite size was 9.7 nm, while the overall CuZnO crystallite size was 17.5 nm; these observations also agree with the FESEM results which found an average CuZnO particle size of 18 nm [41].

It can be seen that the crystallinity of the CuZnO decreases, which may be due to low metal loading and good dispersion [42]. However, this interface between Cu and ZnO species is proposed as the active site and shows promising results for the methanol synthesis step [43].

The N₂ adsorption-desorption isotherms of the HNT, DMF-HNT, 5CZ-PTA@HNT, 10CZ-PTA@HNT, 15CZ-PTA@HNT, and 20CZ-PTA@HNT support and hybrid catalysts, respectively, are presented in (Figure 2). The HNTs were modified with dimethyl formamide (DMF) to improve the dispersion of copper on the surface of the HNTs and prevent the aggregation of CuZnO particles during calcination and reduction. The BET surface area, total pore volume, and pore size results are shown in Table 1. All four catalysts exhibited a typical type IV isotherm with an H₂ hysteresis loop and sudden drop of desorption branch, which is associated with mesoporous materials with bottleneck pores. However, upon closer examination of the findings, there does not seem to be a substantial difference in the textural properties of all the catalysts, apart from a slight decrease in surface area, pore volume, and pore size as the loading of active metal increases. This could be attributed to the blocking of the support's pores. Usually, with traditional impregnation of a metal precursor, the extent of pore narrowing, and surface decrease might increase goes with the bifunctional active sites. However, the PTA acid sites were higher when the metal was small, but acid sites did not contribute to the pore blockage process. The tubular structure of the HNTs was maintained after modification with DMF (see Figure 2; this improved the negatively charged outer surface that allowed for the uniform distribution of CuZnO metal nanoparticles with diameters ranging from 15.6 to 18.4 nm on the outer surface of the HNTs. The process of depositing CuZnO on the outer shell and PTA acid clusters within the lumen of the HNTs after modification with DMF did not significantly affect the mesoporous structure of the support.

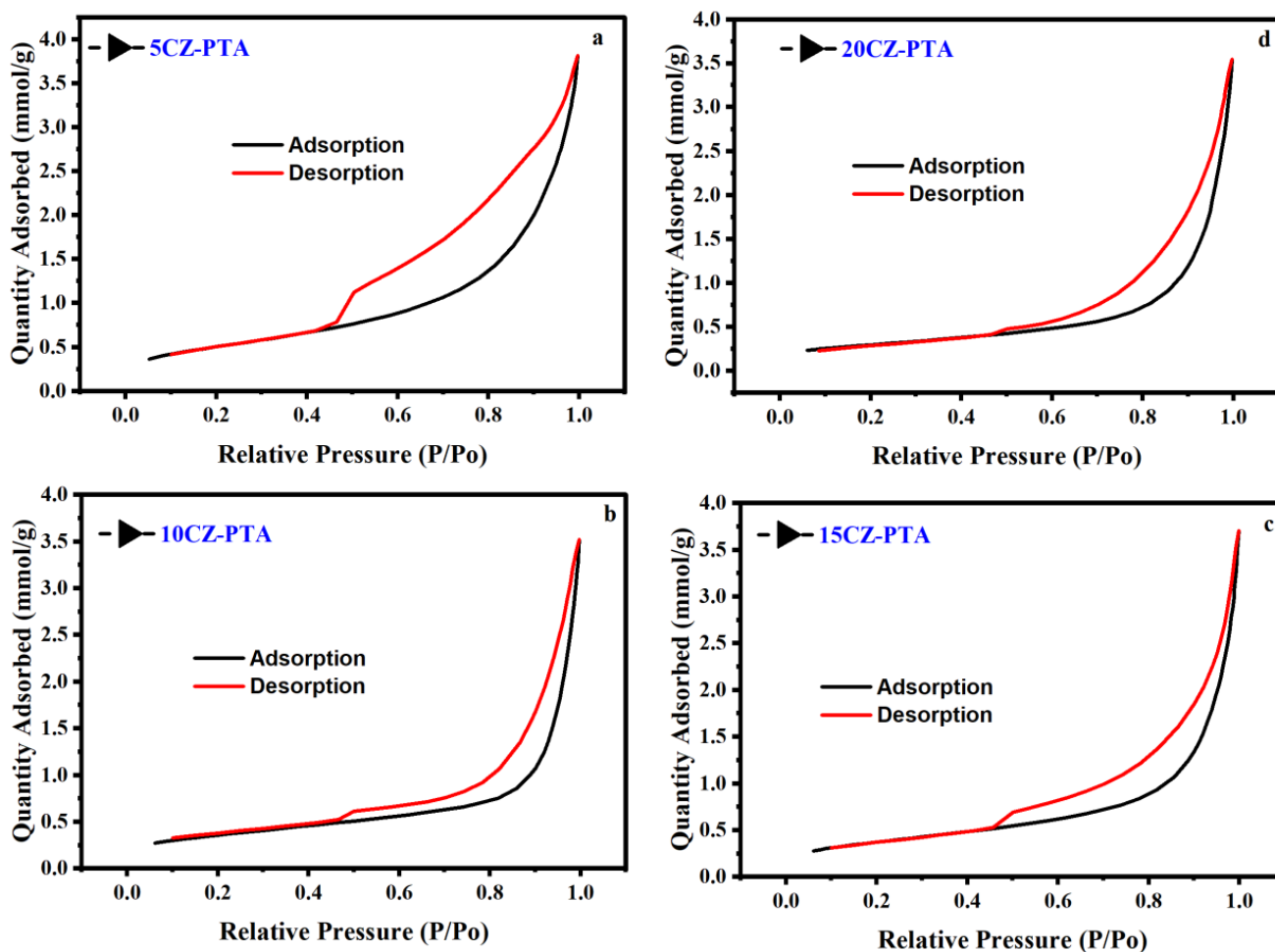


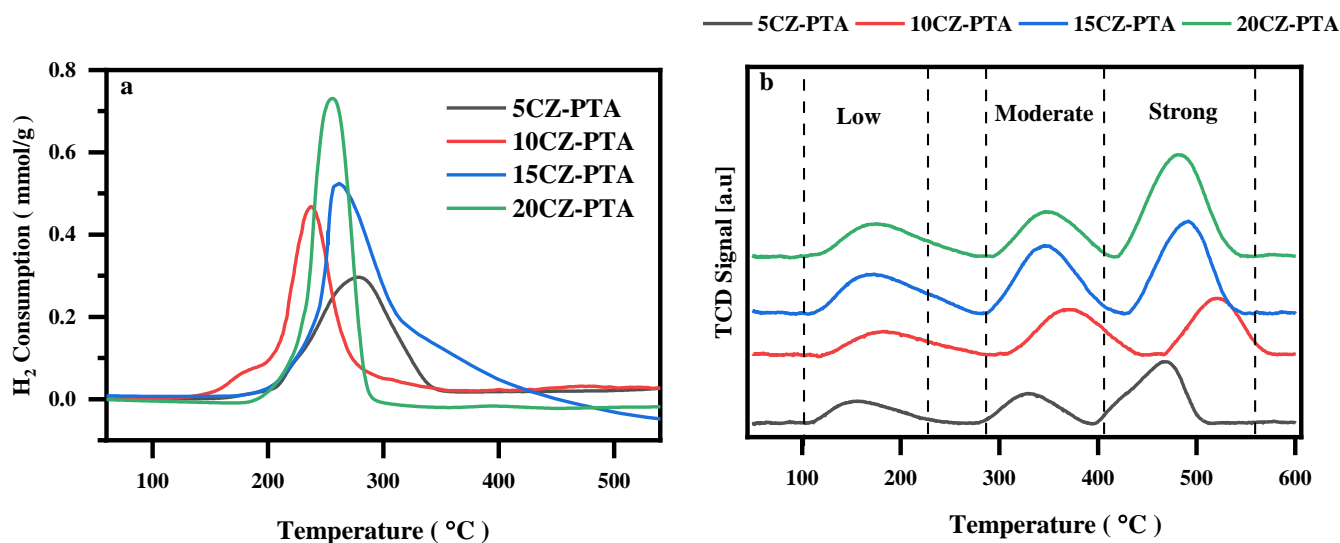
Figure 2. N₂ adsorption-desorption isotherms of (a) 5CZ-PTA@HNT, (b) 10CZ-PTA@HNT (c) 10CZ-PTA@HNT and (d) 20CZ-PTA@HNT.

Table 1. BET, XRD, TPR, and TPD characterization results.

Catalyst Name	BET Surface Area (m ² /g) ^a	Pore Volume (cm ³ /g) ^a	Pore Size (nm) ^a	H ₂ Consumption (mmol/g) ^b	Acidity Distribution (mmol/g) ^c			Cu Crystallite Size (nm) ^d
					Weak	Moderate	Strong	
HNT	65	1.26	15	0	0	0	0	58
HNT-DMF	65.73	0.32	27.8	0	0	0	0	69
20CZ-PTA	21.87	0.110	16	0.731	0.11	0.13	0.25	14.1
15CZ-PTA	23.3	0.11	16.95	0.522	0.17	0.23	0.24	12.3
10CZ-PTA	30	0.116	17.15	0.472	0.20	0.33	0.39	7.6
5CZ-PTA	40	0.133	24.4	0.298	0.21	0.25	0.48	4.8

^a BET nitrogen adsorption method, ^b obtained from H₂-TPR, ^c obtained from TPD-NH₃, ^d obtained from XRD.

Temperature-programmed desorption of ammonia (NH₃-TPD) was used to investigate the acid properties of a hybrid catalyst containing different amounts of 12-phosphotungstic acid (PTA). The results, summarized in (Table 1) and shown in (Figure 3b), indicate that the catalysts exhibited three regions of acid strength based on temperature: weak acid sites at 100–250 °C, medium acid sites at 250–350 °C, and strong acid sites at 350–500 °C. These observations are in line with previous studies showing that the acid strength of PTA increases with increased loading [44]. In general, the acid strength of PTA is expected to increase with increased loading, as a higher concentration of PTA on the catalyst surface should result in a more significant number of strong acid sites. Previous studies have suggested that the strength of the acid sites on the surface of a catalyst can affect the DME selectivity during the reaction. W. Alharbi found a correlation between the turnover rates and catalyst acid strengths for heteropoly acid catalysts; this suggests that the strength of the catalyst acid sites determines the reaction rate [45]. However, it has been reported that weak and medium-strength acid sites are responsible for DME selectivity. In contrast, strong acid sites may accelerate the formation of by-products such as olefins and hydrocarbons [46]. It is important to note that various factors can influence acid site strength, including other species on the active catalyst surface (e.g., co-adsorbed molecules or contaminants) and water formation during the dehydration of methanol to DME. In addition, in some cases, the acid sites may decompose during the reaction, which could affect the catalytic activity and stability; this may be related to the weak interaction between the support and the catalyst [47,48].

**Figure 3.** H₂-TPR profiles of the calcined (a) and NH₃-TPD-profile of reduced (b) CZ-PTA@HNT Catalyst.

The reducibility of calcined hybrid catalysts CZ-PTA was evaluated using the TPR-H₂ technique, as shown in (Figure 3a). The results indicate that within the temperature range of 100–600 °C, only one reduction peak was observed for each catalyst, indicating the degree of reducibility of the metal-support interaction. Interestingly, zinc oxide was found to not reduce within this investigated temperature. On the other hand, Copper samples displayed a broadened peak, while 5CZ and 10CZ showed small shoulder peaks. These reductions in both small and large copper particles can be attributed to the well-dispersed, small loading of CZ, which is indicated by the small peak. Pechenkin et al. [49] reported the same H₂-TPR profile for CuO-In₂O₃ catalysts supported on halloysite nanotube. The reduction profile suggests that hydrogen consumption occurred at a low-temperature range of 150–350 °C, corresponding to the reduction of copper oxide to metallic copper. The amounts of hydrogen consumed by each catalyst are listed in (Table 1).

The TPD-CO₂ techniques were utilized to evaluate the basicity of CZ-PT@HNT reduced catalysts, as shown in Figure 4, through CO₂ desorption profiles. The amount of CO₂ desorbed, and the temperature of desorption provide insight into the basic surface properties of the catalysts. This analysis revealed the presence of two basic sites in all four of the presented HNT-supported CZ-PTA catalysts. The moderate basic sites were attributed to metal–oxygen pairs, such as Cu–O and Zn–O, while the strong basic sites were associated with low-coordination oxygen atoms and O^{2−} ions present at the edge of the crystal structure [28,50]. Desorption of CO₂ at temperatures between 400 and 500 °C corresponded to moderate basic sites, while desorption above 600 °C indicated strong basic sites. The desorption temperature of CO₂ was found to have a strong correlation with the basicity strength of the CZ-PTA@HNT catalysts. The CO₂ desorption profiles were analysed to determine the concentration of basic sites on the catalyst surface by integrating the area of the peak. The balance of active metal sites and solid acid sites largely influenced the overall basicity of the CZ-PTA@HNT catalyst. An increase in Cu metal loading between 5 and 20 wt.% resulted in a rise in the basic site concentration from 0.2681 mmol/g to 0.44029 mmol/g. The literature has reported that the strong basicity of the basic sites in catalysts, although believed to play a crucial role in activating the C–O bond in adsorbed CO₂, may negatively impact the selectivity of dimethyl ether (DME) production. ZnO, being a basic oxide, has been found to partially neutralize the acidity of the catalyst, hindering the transformation of methanol to DME [51]. Mao et al. [52] examined the direct relationship between the methanol dehydration and the nature of the acid sites on HZSM-5 modified with basic oxides, specifically MgO, and discovered that the presence of basic MgO decreased the Brønsted site. The CO₂ adsorption capacity of the 20CZ-PTA@HNT catalyst was found to be the highest among the prepared catalysts, as indicated by its largest desorption peak area with a total of 0.44029 mmol/g. This is due to the presence of 20 wt.% Cu in the catalyst. The basicity of the tested samples was observed to increase in the sequence of 5CZ-PTA@HNT < 10CZ-PTA@HNT < 15CZ-PTA@HNT < 20CZ-PTA@HNT.

The morphological changes of pure HNTs, modified HNTs (DMF-HNTs), and reduced catalysts were investigated using field-emission scanning electron microscope (FESEM) techniques. The study found that most HNT samples retained their tubular geometry; however, some size variations were observed. The external diameter of the HNTs increased after modification from 59 nm to 88, as (Figure 5a,b) shows. In this context, the particle size refers to the physical dimensions of individual particles of the CZ-PTA@HNT catalyst; typically, we have measured the external diameter in nanometres of the HNTs, modified HNTs, CuZnO with the spherical shape of the CZ-PTA@HNT samples using the Image J software.

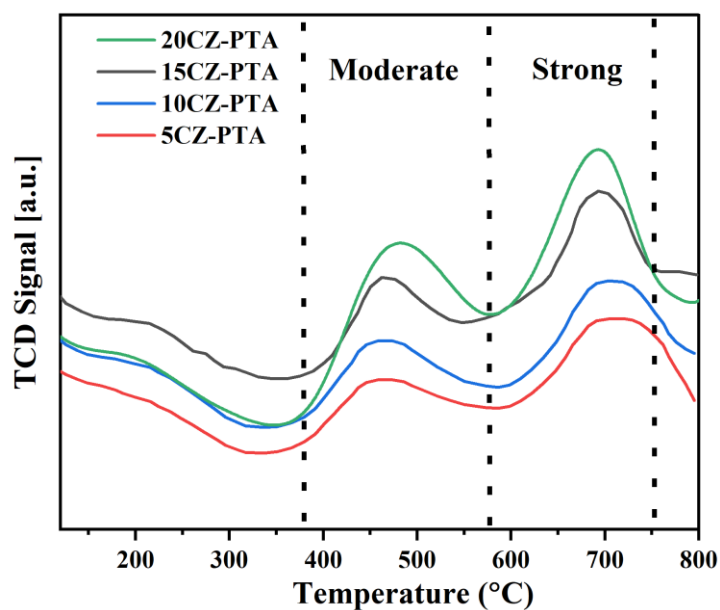


Figure 4. CO₂ temperature-programmed desorption (CO₂-TPD) profiles of the reduced CZ-PTA@HNT catalysts.

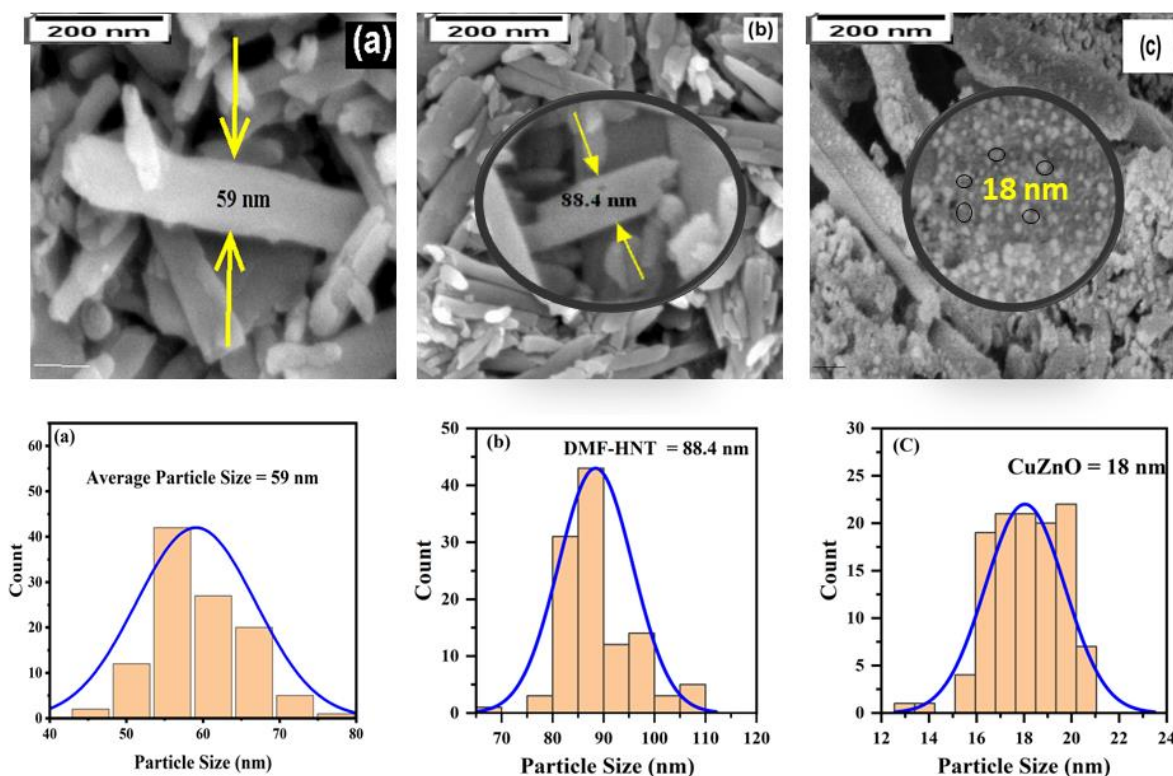


Figure 5. FESEM images of (a) HNT, (b) DMF-HNT, (c) CZ-PTA@HNT, and particle size distribution.

These findings are consistent with those reported by Abdullayev, Elshad, et al., who demonstrated that modification with H₂SO₄ resulted in a 2–3 times enlargement of the lumen diameter of the halloysite. Furthermore, the DMF-modified HNT samples appeared to lose their tubular shape and gradually transform into porous nanorods. These results suggest that modification with both DMF and H₂SO₄ can significantly impact the morphology of HNT samples [34].

At the same time, FESEM also revealed that copper (Cu), copper oxide (Cu_2O), and zinc oxide (ZnO) nanoparticles were uniformly dispersed on the external surface of the halloysite, with an average diameter size of 16–18 nm see (Figure 5c). These nanoparticles were electrostatically deposited on the negative surface of the HNTs, as confirmed by X-ray diffraction (XRD). This combination of Cu(0) or Cu_2O and ZnO nanoparticles resulted from the positive interaction between the HNT outer surface and methanol synthesis active sites [53].

In the preparation process, we theoretically employed Equation (4) to determine the number of active sites loaded on the HNT support. The initial loading varied between 5 and 20 (wt.%) in Cu and PTA. To validate this ratio, we performed EDX analysis with mapping on the calcined CZ-PTA@HNT. The bulk element compositions (Figure 6), displaying the distribution of elemental dots in the CZ-PTA@HNT catalyst. The results indicate a uniform anchoring of Cu, Zn, W, and O on the active sites and detection of Al, Si, and O from the HNT, suggesting even dispersion of CuZnO over the HNT surface. However, the EDX analysis failed to detect phosphorus (P), a PTA solid acid compound component. This may be due to the decomposition of the P during either the calcination or reducing steps.

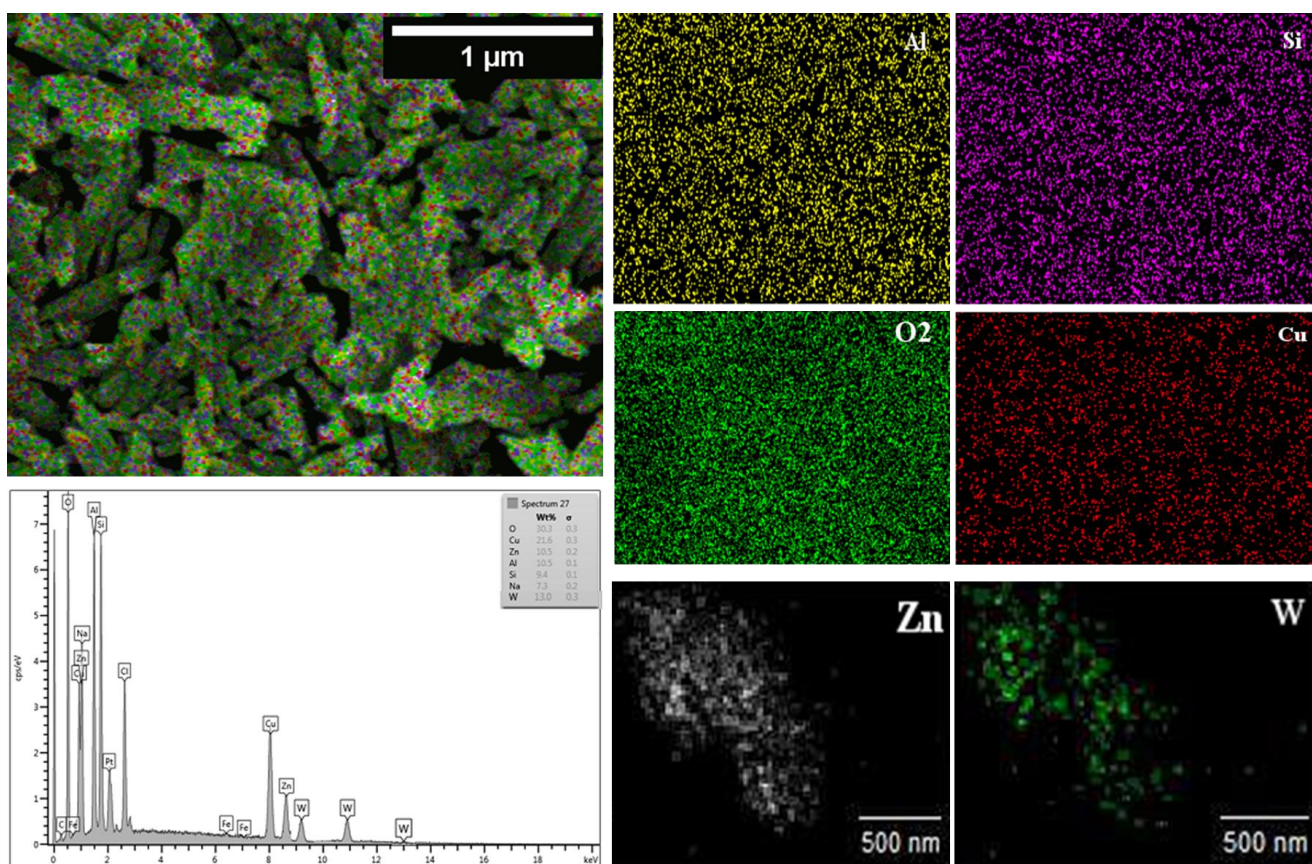


Figure 6. FESEM and EDX elemental mapping images for CZ-PTA@HNT catalyst.

Additionally, this absence may also cause the limitation of the EDX technique. The inaccuracy of the elemental composition may result in the EDX, a surface-sensitive technique that only analyses the top few nanometres of the sample surface. In order to detect elements throughout the entire sample volume, the ICP-MS analysis technique is a better, more sensitive, and more accurate method for elemental analysis than EDX [54].

In conclusion, FESEM and SEM revealed that modification of HNTs with DMF can significantly impact the morphology of the core-shell HNT by altering the lumen diameter, which favors selective loading PTA inside the lumen. Additionally, it has been shown that uniform dispersion of Cu, Cu_2O , and ZnO nanoparticles on the external surface of

halloysite nanotubes can be achieved through a homogeneous nanoparticle distribution. Finally, FESEM and SME also provided valuable insight into the morphological changes of HNTs upon the modification and the unique properties of CuZnO-PTA core-shell nanotube catalyst, which can be utilized to improve the efficient direct synthesis of DME from CO₂ catalytic performance.

The direct synthesis of DME was carried out in a fixed-bed reactor. The reaction conditions were as follows: P = 30 bar, T = 260 °C, H₂/CO₂ = 3:1, Gas Hourly Space Velocity (GHSV) = 12,00 h⁻¹. The products were determined after the reaction reached a steady-state condition, and catalyst performance was evaluated regarding CO₂ conversion and selectivity to products. Furthermore, the amount of H₂O produced in reverse water gas shift reaction RWGSR and methanol dehydration was paid much attention.

The study results displayed in (Table 2) show that the CO₂ conversion slightly increased from 21.47 to 22.36 with the active metal loading, although the difference was relatively small among the four samples tested. This suggests other factors, including catalyst properties, such as the crystallinity, reducibility, dispersion of the CuZnO of the catalyst, and its incorporation to the core-shell structure. For the effective direct synthesis of DME from CO₂ hydrogenation, the catalyst support must possess specific crucial attributes, including a large surface area to support the effective dispersion and reducibility of the active phase. Secondly, the support must be morphologically stable, and thirdly, it should exhibit high mechanical strength. A single core-shell structure can incorporate various active catalytic sites for different reactions. By customizing the core and shell materials to be compatible with sequential reactions, complementary reactions can be conducted in tandem to achieve the desired product conversion [55]. For example, the indirect conversion of CO₂ to DME through the transformation of CO₂ + H₂ into CH₃OCH₃ is a two-step process. The first step involves the conversion of CO₂ and H₂ into MeOH + H₂O as an intermediate via methanol synthesis on the CuZnO active sites of the catalyst, followed by methanol dehydration into DME on the acidic sites of the catalyst PTA. In conventional bifunctional catalysts, typically prepared by physically mixing the active sites, this results in a randomly distributed active site, leading to independent and randomly occurring reactions [56]. However, the non-uniform distribution of active metal sites and acidic sites in conventionally made catalysts can result in intermediates existing for different periods of transport between functions and leading to potential opportunities for undesired reactions, such as CO + H₂. By contrast, core-shell catalysts can potentially mitigate these selectivity limitations by improving the distribution of distances between the separate catalytic sites [25]. Singh, Rajan, and colleagues explored the benefits of using a core-shell configuration for the bifunctional Cu-ZnO-ZrO₂/hierarchical ZSM5 catalyst in hydrogenating CO₂ to methanol and DME. The results showed that the core-shell design allowed for the physical separation of the environments of the methanol synthesis and its conversion into DME reactions, enhancing their synergetic interaction [57]. The effectiveness of a catalyst in direct CO₂ hydrogenation to DME depends heavily on its characteristics. A promoter such as ZnO, which has redox properties, can improve the catalyst's performance by facilitating the dispersion and reducing properties of the Cu active site [58]. Although Cu can work alone as a catalyst for making methanol, its activity is usually boosted by interacting with ZnO, which has almost no catalytic activity on its own [59]. The interaction between Cu and ZnO can influence the metal site's reactivity and redox properties. When oxygen vacancies are present, the surface becomes electron-rich, enhancing its electron-donating ability and making it more active in adsorbing hydrogen [60]. The ZnO surface was significant as it had a high concentration of dispersed Cu atoms and a strong interaction between Cu and the surface. This created active sites for the hydrogenation of CO₂. On the other hand, when H₂ adsorbed on the oxygen vacancy on the Cu-ZnO surface, it would release a proton to a nearby oxygen atom, forming two hydroxyl groups for each vacancy. Meanwhile, CO₂ acts as a Lewis acid and the zinc vacancies on the surface serve as active Lewis basic sites for Lewis acid-base interactions [61,62].

Table 2. CZ-PTA@HNT catalyst performance in direct synthesis of DME from CO₂ hydrogenation.

Catalyst	CO ₂ Conversion, %	DME Selectivity, %	MeOH Selectivity, %	CO Selectivity, %	H ₂ O Selectivity, %
20CZ-PTA	22.36	52	18	22.7	2.6
15CZ-PTA	21.4	56.6	16.7	20.5	4.3
10CZ-PTA	23.45	62.3	15	17.5	6.8
5CZ-PTA	21.47	68.9	7	15.3	8.2

Reaction conditions: P = 30 bar, T = 260 °C, H₂/CO₂ = 3:1, Gas Hourly Space Velocity (GHSV) = 12,00 h⁻¹; time on = 300 min.

In addition, the presence of water formed by RWGSR may significantly impact the conversion rate. However, RWGSR Equation (2) is considered the most challenging aspect in directly converting CO₂ to DME because it causes severe deactivation of the Cu metal active site [46]. To efficiently convert CO₂ into DME over a CuZnO-PTA catalyst, it is important to understand the two main pathways, RWGS (via HOCO intermediate) and the formate (via HCOO intermediate) pathways [63]. Understanding these mechanisms can optimize the catalyst's performance and prevent early deactivation. Yixiong Yang et al. investigated methanol synthesis via CO₂ hydrogenation over various Cu nanoparticles (NPs), focusing on determining the reaction pathways involved. Through a combination of experimental techniques and density functional theory (DFT) calculations, they concluded that reaction (2) undergoes a formate intermediate [64]. In this study, we observed RWGSR selectivity decreases with an increase in Cu metal loading from 5 to 20 wt%, and the H₂-TPR data confirmed that Cu reduction strength increased with Cu loading; this may contribute to the suppression of the RWGSR reaction by changing the reaction pathway from decomposition cleavage of CO₂ to CO* + O* via the direct C-O bond cleavage pathway to the more reactive carboxyl (COOH*) or formate (HCOO*) intermediates [65].

The effect of PTA wt% loaded inside the HNT lumen on the catalytic activity, and product selectivity was evaluated in the range of 5 wt% to 20 wt% as (Figure 7a) shows. The selectivity to DME of all catalysts significantly increased with increasing the PTA loading, which can be explained by the fact that DME's selectivity depends on the methanol dehydration reaction (3) driven by acid strength. Similarly, previous studies have reported the relationship between Bronsted acid clusters of heteropoly acid catalysts and DME selectivity. Rawan Al-Faze and his co-workers have investigated the effect of silica-supported heteropoly acids loading and acid strength on methanol dehydration and DME selectivity; they have reported similar observations in their experiments [66]. As we know, the methanol dehydration step in Equation (3) prefers low and moderate acid strength to achieve high selectivity of DME compared to stronger acid sites. Ladera, Rosa María, et al. studied methanol dehydration to DME over silica HSiW and tungstic HPW heteropoly acid supported on TiO₂. They concluded that DME selectivity strongly depends on HPA loading on TiO₂, and it has been found that the optimum acid site loading was 2.3 Keggin units per nm² after it was well dispersed on the TiO₂ [49]. In summary, acid site strength optimization is important in the methanol dehydration to DME reaction because it can help to achieve high selectivity and high conversion, improve the long-term performance and stability of the catalyst, and reduce the formation of by-products.

Moreover, methanol selectivity decreased with PTA loading while water selectivity increased (Figure 7a). As we know, the DME synthesis from CO₂ hydrogenation contains two water-generating reactions, methanol dehydration and reverse water gas shift reaction; the water formed may cause severe deactivation to both active sites of the hybrid catalyst. In this regard, despite the increased selectivity towards the water with increased loading of PTA, the catalyst exhibited outstanding activity and resilience towards water produced during the methanol dehydration step. This can be attributed to the unique properties of the Brønsted acid sites present in PTA, as opposed to other solid acid catalysts with Lewis acid sites, such as γ-Al₂O₃, which tend to adsorb water, leading to a substantial decrease in the number of acid sites and, ultimately, catalyst deactivation [67,68].

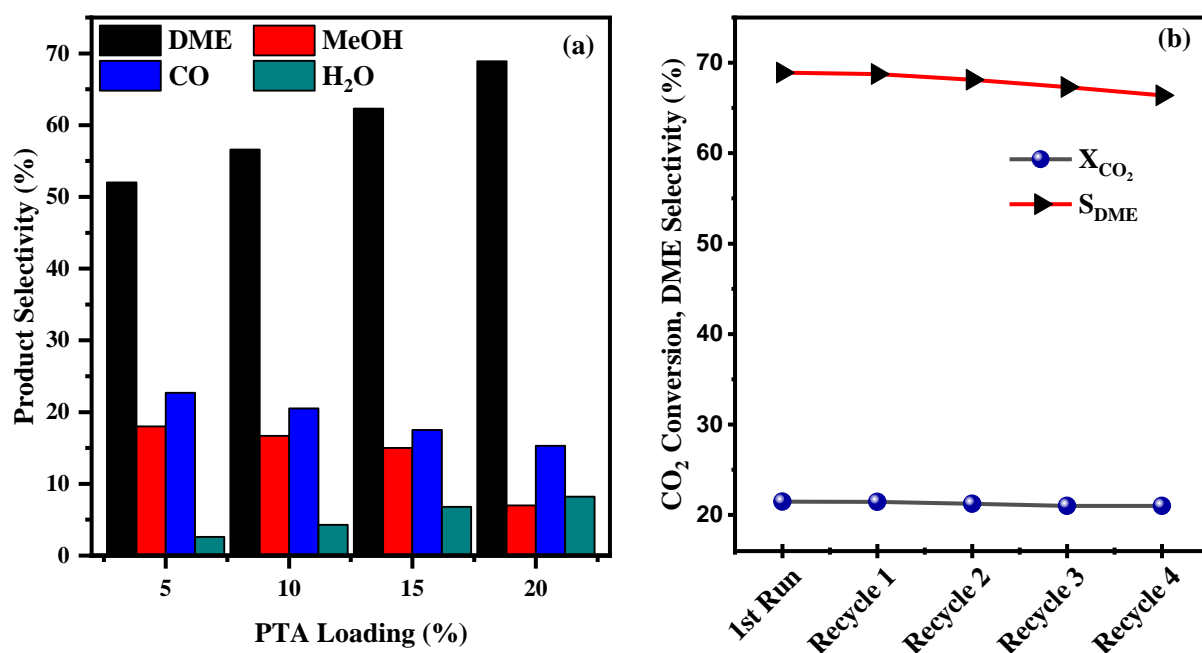


Figure 7. Effect of PTA loading (wt.%) on product selectivity of DME, MeOH, CO, and H₂O (a), and (b) stability test by recycling the 5CZ-PTA@HNT catalyst on CO₂ conversion and DME selectivity.

In the direct conversion of CO₂ into DME, the reaction temperature has crucial influences on the catalytic performance of the CZ-PTA@HNT catalyst. The temperature varied from 180 °C to 320 °C at a constant pressure of 30 bar, GHSV of 12,000 h⁻¹, and a catalyst weight of 0.3 g. The results showed that CO₂ conversion increased with temperature from 12.36% to 26.92%, and DME selectivity increased from 2.4% until maximum DME selectivity of 68.9% was achieved at 260 °C (Table 3). The decrease in DME selectivity at higher temperatures was predictable from a thermodynamic perspective. The DME synthesis reaction is reversible and exothermic. Its equilibrium conversion decreases significantly at higher temperatures, leading to a decrease in DME selectivity, highlighting the importance of controlling the temperature in this reaction [69]. Operating at less than 305 °C provides a good compromise between CO₂ conversion and DME selectivity, as higher reaction temperatures have an unfavorable effect on oxygenate yield and selectivity, such as MeOH and DME, according to reported findings by Ateka, Ainara, et al. [11].

Table 3. Effect of reaction temperature on CO₂ conversion and product selectivity over 5CZ-PTA@HNT.

Temperature (°C)	CO ₂ Conversion, %	DME Selectivity, %	MeOH Selectivity, %	CO Selectivity, %	H ₂ O Selectivity, %
180	12.36	2.4	36.54	48.7	4.6
220	18.27	32.6	16.7	27.6	9.3
260	21.47	68.9	7	15.3	8.2
300	26.18	64.7	12	18.3	12.6
320	26.92	48.11	18.15	39.43	15.52

Reaction conditions: P = 30 bar, H₂/CO₂ = 3:1, GHSV = 12,00 h⁻¹; time = 300 min, (0.3 g catalyst).

In addition to improving CO₂ conversion, the increase in temperature also led to higher H₂O and CO selectivity due to the thermodynamic advantage of the reverse water-gas shift reaction at higher temperatures [70]. This highlights the complexity of the reaction system and the interplay between different reactions, making it crucial to consider thermodynamics and kinetics to optimize the process. In conclusion, the study highlights the crucial role of

temperature in the direct conversion of CO₂ into DME. In order to understand and provide valuable insights into this reaction, the thermodynamic and kinetic aspects of the reaction system should be investigated in the future.

The reusability of the 5CZ-PTA@HNT catalyst was evaluated through consecutive continuous mode in a fixed bed reactor at optimized temperature (260 °C), pressure (30 bar), GHSV (12,00 h⁻¹), and catalyst weight (0.3 g). The first reaction was labeled as (Run 1) and was carried out using a fresh catalyst, as shown in (Figure 7b). The catalyst was kept in the reactor and reused for subsequent experiments (Recycle 1 to Recycle 4) under the same reaction conditions; each run was studied for 3 h. The results showed good stability throughout the recycling process, with CO₂ conversion and DME selectivity remaining steady at around 21.47% and 68.9%, respectively, for five consecutive cycles. No significant decrease in CO₂ conversion and DME selectivity was observed during the 15 h total reaction duration, demonstrating that this enhanced catalyst can continuously operate with good activity and stability. The reusability study also showed that CO₂ conversion and DME selectivity remained unchanged. The catalyst can be easily recovered and reused without significantly reduced catalytic performance. Hence, the CZ-PTA@HNT catalyst is considered a promising candidate for industrial application.

3. Materials and Methods

3.1. Catalyst Preparation

Halloysite nano clay (Al₂Si₂O₅(OH)₄·2H₂O), Tungstophosphoric acid (H₃[P(W₃O₁₀)₄]·xH₂O), copper nitrate trihydrate (Cu(NO₃)₂·3H₂O), and zinc nitrate tetrahydrate (Zn(NO₃)₂·4H₂O) were used in this study as the precursors for the catalyst preparation. These materials and Dimethylformamide (HCON(CH₃)₂) were purchased from Sigma-Aldrich. To synthesize the CuZnO/PTA@HNT core-shell bi-functional catalyst with different mass ratios of Cu/PTA, the halloysite nanotube (HNT) was first modified by intercalating it with Dimethylformamide (DMF) to increase the HNT's surface charges, interlayer spacing, and inner lumen size. This was achieved by: (a) drying 20 g of HNT overnight at 110 °C; (b) adding 10 g of the dried HNT to 100 mL of DMF while stirring continuously at 60 °C; and (c) rinsing the HNT-DMF several times with a solution containing distilled water and 30% ethanol before drying it for 48 h in an air oven at 80 °C. Then, the co-impregnation incipient wetness method was used to prepare the bifunctional catalyst. Methanol synthesis (CuZnO) and methanol dehydration (PTA) dual-sites were co-impregnated onto the support (HNT) to synthesize the CuZn-PTA@HNT core-shell nanotube bi-functional catalyst. Specifically, the precursors of active metal Cu, promoter ZnO, and solid acid PTA were dissolved in deionized water (DW) and added drop by drop to the appropriate amount of HNT suspended in a beaker with DW. The amount of active metal used as weight (%) was calculated using Equation (4). The slurry was then stirred for 24 h at 65 °C, and the obtained solid was dried overnight before being calcined in a dry air oven at 350 °C for four hours.

$$\text{Cu(NO}_3)_2 \cdot 3\text{H}_2\text{O required (g)} = \text{Amount of Cu required (g)} \times \frac{1 \text{ mol Cu}}{63.546 \text{ g}} \times \frac{1 \text{ mol Cu} \times 241.60 \text{ g}}{1 \text{ mol Cu(NO}_3)_2 \cdot 3\text{H}_2\text{O}} \quad (4)$$

3.2. Catalyst Characterisation

A Shimadzu XRD 600 X-ray diffractometer (XRD) with Cu target K radiation at 30 kV and 30 mA examined the reduced catalysts' crystalline structure, phase, and textural features. Diffractograms were generated at a scanning speed of 1 degree per minute using a scanning angle (2theta) of 5 to 100 degrees. First, the reduced catalyst was pressed flat in a plastic sample holder before being scanned with an X-ray machine for defects. Next, an X-ray line broadening at the metallic Cu's most intense peak was used to determine the crystalline size of the metal.

Next, reduced catalyst morphology and elementary surface composition were characterised using Hitachi's cold field emission technology with double condenser optics and superb resolution with complete control of the probe current from 1 pA to more than 5 nA

elemental analysis EDX-ray spectroscopy (Oxford Xmax 50 mm). In addition, a voltage accelerator with a scanning power of 2.0 kV and a secondary electron detector with a range of magnifications (5K \times , 20K \times , 30K \times , 50K \times , 60K \times , 80K \times) were utilised to enhance the image resolution.

The textural properties, including surface area and porosity of the catalyst, were measured using the multiple-point surface area analyser TriStar II 3020 Version 3.02. Finally, 0.2 g of the reduced catalyst was degassed for 2 h at 200 °C in an H₂ environment to eliminate all gases and moisture adsorbed from the atmosphere. The N₂ physisorption was carried out at a temperature of liquid N₂ (77.350 K) over a relative pressure (p/p_0) and an equilibration interval of 10 s. The surface area, pore volume, and pore size were determined using different techniques, including single point, BET, Langmuir, t-Plot, and BJH Adsorption, with the cumulative surface area pore between 1.7 nm and 300 nm in diameter.

The chemisorption of the reduced catalyst was studied via Micromeritics Chemisorb 2720 chemisorption. First, the total acidity and basicity were measured by temperature-programmed desorption of ammonia and CO₂ (NH₃, CO₂-TPD). Next, 20 mg of the catalyst was treated with pure He flows of 20 mL/min at 150 °C for 45 min to remove moisture and other impurities. Next, the sample was cooled down to room temperature, and then a base probe (5% NH₃ in H₂) was saturated for 30 min before purging the sample H₂ gas at 100 °C to remove physisorbed NH₃ or CO₂. Finally, the desorption process was started by ramping the temperature at a 10 °C/min rate until it reached 900 °C.

Then, the temperature-programmed desorption profile was obtained to calculate the catalyst's surface acid and base strength as also total acidity and basicity. Then, using the same chemisorption analyser (Micromeritics Chemisorb 2720) with a thermal conductivity detector (TCD), we were able to estimate the optimum reduction temperature and the reducibility of the active metal (Cu). In addition, to ensure that the catalyst surface was free of moisture and impurities before the reduction process, the catalyst sample was degassed at 200 °C for 30 min in pure helium (He) at a flow rate of 20 mL/min. Finally, a temperature ramping rate of 20 °C/min under atmospheric pressure was used to heat the catalyst in a U-shaped reactor to obtain the H₂-TPR profile. As a result, reduced gas (H₂) is purged through the catalyst at a flow rate of 20 mL/min for the duration of the reduction process.

3.3. Catalyst Performance in CO₂ Hydrogenation to DME

The catalytic activity of the prepared CZ-PTA core-shell nanotube was performed in differential a fixed bed stainless steel tubular reactor of 150 mm length \times 1/4 inch inner diameter; the catalyst bed was placed in the bottom of the tube with a diameter of 1/8 inch. Lindberg/Blue M™ Mini-Mite™ Tube Furnaces were used to heat the reactor, and for temperature monitoring, a K-type thermocouple was installed above the catalyst bed. In addition, 0.3 g of the catalyst sample was placed on stainless steel mesh located in the heated zone of the reactor. Before the experiment, the catalyst was reduced with a pure H₂ flow of 20 mL/min at 400 °C for 3 h. Subsequently, the reactor was set to the desired reaction temperature. Then, CO₂ hydrogenation reaction was carried out at 260 °C, 30 bar, GHSV of 12,000 h⁻¹ and CO₂/H₂ 1:3 ratio. Finally, the composition products were analysed using Agilent J&W HP-PLOT Q capillary column installed in gas chromatography (Agilent 6890N) for oxygenates such as MeOH, CH₃OCH₃, and SRI Model 8610C GC equipped with 60/80 Carboxen-1000 packing column to separate permanent gases (CO₂, CO, H₂, CH₄) and hydrocarbon; both GC used TCD thermal conductivity detector (TCD). The GC was programmed at 40 °C for 4 min, then increased to 180 °C at 20 °C/min and held for 5 min. The carrier gas flow rate (He) was 40 mL/min. For each run, the sample was collected every 25 min; five samples were collected for every catalyst performance test, and the average data was reported. The CO₂ conversion (XCO₂), product selectivity (DME, CO, Methanol, and H₂O), and product analysis were calculated based on Equations (5)–(9).

$$X_{CO_2} = \frac{F_{CO_{2in}} - F_{CO_{2out}}}{F_{CO_{2in}}} \quad (5)$$

$$\text{DME Selectivity} = \frac{2 * F_{DME}}{F \text{ CO}_{2in} - F \text{ CO}_{2out}} \quad (6)$$

$$\text{CH}_3\text{OH Selectivity} = \frac{F_{MeOH}}{F \text{ CO}_{2in} - F \text{ CO}_{2out}} \quad (7)$$

$$\text{CO Selectivity} = \frac{F_{MeOH}}{F \text{ CO}_{2in} - F \text{ CO}_{2out}} \quad (8)$$

$$\text{H}_2\text{O Selectivity} = \frac{F \text{ H}_2\text{O}}{F \text{ CO}_{2in} - F \text{ CO}_{2out}} \quad (9)$$

where F (mol/min) represents the molar flow rate of the reactants and products in the reaction.

4. Conclusions

This study aimed to develop a dual-functional, halloysite nanotube-supported CuZnO-PTA catalyst with a core-shell structure and investigate the effects of the active site mass ratio CuZnO/PTA on CO₂ conversion and DME selectivity. CuZnO-PTA hybrid core-shell nanotube catalysts with a different ratio of Cu/PT were prepared by impregnation and supported on modified aluminosilicate HNTs. The catalytic activity of the CuZnO-PTA@HNT was studied in CO₂ hydrogenation to DME. Based on data from physicochemical methods, such as XRD, SBET, FESEM, TPD-NH₃, and H₂-TPR, we can surmise that these catalysts have two types of active sites—Cu particles, which are responsible for methanol formation, and acid sites of PTA, which are responsible for methanol dehydration to DME. The influence of the Cu/PTA mass ratio was studied. The CO₂ was almost the same for all four catalysts, which provided 23% CO₂ conversion with a DME selectivity of 68%.

Furthermore, it was shown that DME selectivity depends on the acidity of the catalyst, and the catalyst poses high resistance toward the water formed. In addition, this study highlights the crucial role of temperature in the direct conversion of CO₂ into DME. The results show that increasing the temperature improves CO₂ conversion but decreases DME selectivity. A temperature of less than 305 °C is a good compromise between CO₂ conversion and DME selectivity. The study also emphasizes the importance of considering thermodynamics and kinetics to optimize the process. The reusability of the CZ-PTA@HNT catalyst was evaluated and showed good stability and continuous activity/stability over five consecutive cycles. The catalyst is considered a promising candidate for industrial application due to its high performance and easy recovery and reuse.

This study has demonstrated the effectiveness of using mesoporous HNTs as support for CuZnO metal nanoparticles in directly synthesising DME from CO₂ hydrogenation. The use of HNTs as a support not only improved the stability and activity of the CuZnO catalysts but also prevented the aggregation of CuZnO nanoparticles, which is a common issue in this reaction. This was achieved through the modification of HNTs with DMF, which increased the dispersion of copper on the outer surface of the HNTs and resulted in a uniform distribution of CuZnO nanoparticles. The resulting CZ-PTA/HNT catalysts showed high conversion and selectivity towards DME, with the 20CZ-PTA/HNT catalyst achieving the highest DME selectivity of 63.3 mol%. One potential area for future research could be exploring these modified HNTs as support for other types of catalysts, such as those used in CO₂ methanation to fuels and chemicals. Finally, the study found that temperature plays a critical role in converting CO₂ into DME. Optimal results were obtained at less than 305 °C, balancing CO₂ conversion and DME selectivity. The 5CZ-PTA@HNT catalyst showed good stability and reusability with consistent results over five cycles.

One limitation of this research is that it focused solely on using DFM as a modifying agent for the HNTs. It would be beneficial to explore the use of other modifying agents to see if similar or improved results can be achieved. Additionally, the study is based on a limited number of runs (five consecutive cycles), so it would be interesting to investigate the long-term stability and durability of these modified HNTs under reaction conditions, as this is an essential factor in their potential practical application.

Author Contributions: Methodology, M.Y.M., A.A. (Arshad Ahmad), M.L.P.P., T.A.T.A., A.A. (Afizah Alir); software, M.Y.M., W.N.; resources, T.A.T.A., A.A. (Arshad Ahmad), M.I.; data curation, W.N., T.A.T.A.; writing—original draft preparation, M.Y.M.; writing—review and editing, M.I., W.N., A.A. (Arshad Ahmad); supervision, T.A.T.A.; funding acquisition, T.A.T.A., W.N. All authors have read and agreed to the published version of the manuscript.

Funding: This research was funded by the Malaysia Ministry of Higher Education.

Data Availability Statement: The data supporting this study's findings are available within the article. In addition, data can also be obtained upon request from the corresponding author.

Acknowledgments: The authors are grateful for the support given by Universiti Teknologi Malaysia (UTM) allocation budget in Pusat Pengurusan Makmal Universiti (PPMU) laboratory. W. Nabgan is thankful for the support from Universitat Rovira i Virgili under the Maria Zambrano Programme (Reference number: 2021URV-MZ-10).

Conflicts of Interest: The authors declare no conflict of interest.

References

1. Navarro-Jaén, S.; Virginie, M.; Thuriot-Roukos, J.; Wojcieszak, R.; Khodakov, A.Y. Structure–performance correlations in the hybrid oxide-supported copper–zinc SAPO-34 catalysts for direct synthesis of dimethyl ether from CO₂. *J. Mater. Sci.* **2022**, *57*, 3268–3279. [[CrossRef](#)]
2. D'Alessandro, D.M.; Smit, B.; Long, J. Carbon dioxide capture: Prospects for new materials. *Angew. Chem. Int. Ed. Engl.* **2010**, *49*, 6058–6082. [[CrossRef](#)] [[PubMed](#)]
3. Mota, N.; Millán Ordoñez, E.; Pawelec, B.; Fierro, J.L.G.; Navarro, R.M. Direct Synthesis of Dimethyl Ether from CO₂: Recent Advances in Bifunctional/Hybrid Catalytic Systems. *Catalysts* **2021**, *11*, 411. [[CrossRef](#)]
4. Kornas, A.; Śliwa, M.; Ruggiero-Mikołajczyk, M.; Samson, K.; Podobiński, J.; Karcz, R.; Duraczyńska, D.; Rutkowska-Zbik, D.; Grabowski, R. Direct hydrogenation of CO₂ to dimethyl ether (DME) over hybrid catalysts containing CuO/ZrO₂ as a metallic function and heteropolyacids as an acidic function. *React. Kinet. Mech. Catal.* **2020**, *130*, 179–194. [[CrossRef](#)]
5. Whang, H.S.; Lim, J.; Choi, M.S.; Lee, J.; Lee, H. Heterogeneous catalysts for catalytic CO₂ conversion into value-added chemicals. *BMC Chem. Eng.* **2019**, *1*, 9. [[CrossRef](#)]
6. Mondal, U.; Yadav, G.D. Perspective of dimethyl ether as fuel: Part I. Catalysis. *J. CO₂ Util.* **2019**, *32*, 299–320. [[CrossRef](#)]
7. Arcoumanis, C.; Bae, C.; Crookes, R.; Kinoshita, E. The potential of dimethyl ether (DME) as an alternative fuel for compression-ignition engines: A review. *Fuel* **2008**, *87*, 1014–1030. [[CrossRef](#)]
8. Boon, J.; van Kampen, J.; Hoogendoorn, R.; Tanase, S.; van Berkel, F.P.F.; van Sint Annaland, M. Reversible deactivation of γ -alumina by steam in the gas-phase dehydration of methanol to dimethyl ether. *Catal. Commun.* **2019**, *119*, 22–27. [[CrossRef](#)]
9. Aloise, A.; Marino, A.; Dalena, F.; Giorgianni, G.; Migliori, M.; Frusteri, L.; Cannilla, C.; Bonura, G.; Frusteri, F.; Giordano, G. Desilicated ZSM-5 zeolite: Catalytic performances assessment in methanol to DME dehydration. *Microporous Mesoporous Mater.* **2020**, *302*, 110198. [[CrossRef](#)]
10. Kattel, S.; Ramírez, P.J.; Chen, J.G.; Rodriguez, J.A.; Liu, P. Active sites for CO₂ hydrogenation to methanol on Cu/ZnO catalysts. *Science* **2017**, *355*, 1296–1299. [[CrossRef](#)]
11. Ateka, A.; Sánchez-Contador, M.; Portillo, A.; Bilbao, J.; Aguayo, A.T. Kinetic modeling of CO₂+CO hydrogenation to DME over a CuO-ZnO-ZrO₂@SAPO-11 core-shell catalyst. *Fuel Process. Technol.* **2020**, *206*, 106434. [[CrossRef](#)]
12. Mao, D.; Zhang, J.; Zhang, H.; Wu, D. A highly efficient Cu-ZnO/SBA-15 catalyst for CO₂ hydrogenation to CO under atmospheric pressure. *Catal. Today* **2022**, *402*, 60–66. [[CrossRef](#)]
13. Lin, L.; Yao, S.; Liu, Z.; Zhang, F.; Li, N.; Vovchok, D.; Martínez-Arias, A.; Castañeda, R.; Lin, J.; Senanayake, S.D.; et al. In Situ Characterization of Cu/CeO₂ Nanocatalysts for CO₂ Hydrogenation: Morphological Effects of Nanostructured Ceria on the Catalytic Activity. *J. Phys. Chem. C* **2018**, *122*, 12934–12943. [[CrossRef](#)]
14. Krim, K.; Sachse, A.; Le Valant, A.; Pouilloux, Y.; Hocine, S. One Step Dimethyl Ether (DME) Synthesis from CO₂ Hydrogenation over Hybrid Catalysts Containing Cu/ZnO/Al₂O₃ and Nano-Sized Hollow ZSM-5 Zeolites. *Catal. Lett.* **2022**, *153*, 83–94. [[CrossRef](#)]
15. Peinado, C.; Liuzzi, D.; Retuerto, M.; Boon, J.; Peña, M.A.; Rojas, S. Study of catalyst bed composition for the direct synthesis of dimethyl ether from CO₂-rich syngas. *Chem. Eng. J. Adv.* **2020**, *4*, 100039. [[CrossRef](#)]
16. Argyle, M.; Bartholomew, C. Heterogeneous Catalyst Deactivation and Regeneration: A Review. *Catalysts* **2015**, *5*, 145–269. [[CrossRef](#)]
17. Torres-Linan, J.; Ruiz-Rosas, R.; Rosas, J.M.; Rodriguez-Mirasol, J.; Cordero, T. A Kinetic Model Considering Catalyst Deactivation for Methanol-to-Dimethyl Ether on a Biomass-Derived Zr/P-Carbon Catalyst. *Materials* **2022**, *15*, 596. [[CrossRef](#)]
18. Cai, Z.; Dai, J.; Li, W.; Tan, K.B.; Huang, Z.; Zhan, G.; Huang, J.; Li, Q. Pd Supported on MIL-68(In)-Derived In₂O₃ Nanotubes as Superior Catalysts to Boost CO₂ Hydrogenation to Methanol. *ACS Catal.* **2020**, *10*, 13275–13289. [[CrossRef](#)]
19. Asthana, S.; Samanta, C.; Bhaumik, A.; Banerjee, B.; Voolapalli, R.K.; Saha, B. Direct synthesis of dimethyl ether from syngas over Cu-based catalysts: Enhanced selectivity in the presence of MgO. *J. Catal.* **2016**, *334*, 89–101. [[CrossRef](#)]

20. Cai, M.; Palčić, A.; Subramanian, V.; Moldovan, S.; Ersen, O.; Valtchev, V.; Ordonsky, V.V.; Khodakov, A.Y. Direct dimethyl ether synthesis from syngas on copper–zeolite hybrid catalysts with a wide range of zeolite particle sizes. *J. Catal.* **2016**, *338*, 227–238. [[CrossRef](#)]
21. Moradi, G.R.; Nosrati, S.; Yaripor, F. Effect of the hybrid catalysts preparation method upon direct synthesis of dimethyl ether from synthesis gas. *Catal. Commun.* **2007**, *8*, 598–606. [[CrossRef](#)]
22. Guzmán, H.; Roldán, D.; Russo, N.; Hernández, S. Ultrasound-assisted synthesis of copper-based catalysts for the electrocatalytic CO₂ reduction: Effect of ultrasound irradiation, precursor concentration and calcination temperature. *Sustain. Mater. Technol.* **2023**, *35*, e00557. [[CrossRef](#)]
23. Li, H.; Zhang, P.; Guo, L.; He, Y.; Zeng, Y.; Thongkam, M.; Natakaranakul, J.; Kojima, T.; Reubroycharoen, P.; Vitidsant, T.; et al. A Well-Defined Core-Shell-Structured Capsule Catalyst for Direct Conversion of CO₂ into Liquefied Petroleum Gas. *ChemSusChem* **2020**, *13*, 2060–2065. [[CrossRef](#)] [[PubMed](#)]
24. Rusdan, N.A.; Timmiati, S.N.; Isahak, W.N.R.W.; Yaakob, Z.; Lim, K.L.; Khaidar, D. Recent Application of Core-Shell Nanostructured Catalysts for CO₂ Thermocatalytic Conversion Processes. *Nanomaterials* **2022**, *12*, 3877. [[CrossRef](#)]
25. Das, S.; Perez-Ramirez, J.; Gong, J.; Dewangan, N.; Hidajat, K.; Gates, B.C.; Kawi, S. Core-shell structured catalysts for thermocatalytic, photocatalytic, and electrocatalytic conversion of CO₂. *Chem. Soc. Rev.* **2020**, *49*, 2937–3004. [[CrossRef](#)]
26. Karaman, B.P.; Oktar, N.; Doğu, G.; Dogu, T. Heteropolyacid Incorporated Bifunctional Core-Shell Catalysts for Dimethyl Ether Synthesis from Carbon Dioxide/Syngas. *Catalysts* **2022**, *12*, 1102. [[CrossRef](#)]
27. Sánchez-Contador, M.; Ateka, A.; Aguayo, A.T.; Bilbao, J. Direct synthesis of dimethyl ether from CO and CO₂ over a core-shell structured CuO-ZnO-ZrO₂@SAPO-11 catalyst. *Fuel Process. Technol.* **2018**, *179*, 258–268. [[CrossRef](#)]
28. Yang, H.; Gao, P.; Zhang, C.; Zhong, L.; Li, X.; Wang, S.; Wang, H.; Wei, W.; Sun, Y. Core-shell structured Cu@m-SiO₂ and Cu/ZnO@m-SiO₂ catalysts for methanol synthesis from CO₂ hydrogenation. *Catal. Commun.* **2016**, *84*, 56–60. [[CrossRef](#)]
29. Sánchez-Contador, M.; Ateka, A.; Ibáñez, M.; Bilbao, J.; Aguayo, A.T. Influence of the operating conditions on the behavior and deactivation of a CuO-ZnO-ZrO₂@SAPO-11 core-shell-like catalyst in the direct synthesis of DME. *Renew. Energy* **2019**, *138*, 585–597. [[CrossRef](#)]
30. Cui, X.; Chen, S.; Yang, H.; Liu, Y.; Wang, H.; Zhang, H.; Xue, Y.; Wang, G.; Niu, Y.; Deng, T.; et al. Improving methanol selectivity in CO₂ hydrogenation by tuning the distance of Cu on catalyst. *Appl. Catal. B Environ.* **2021**, *298*, 120590. [[CrossRef](#)]
31. Lvov, Y.; Panchal, A.; Fu, Y.; Fakhrullin, R.; Kryuchkova, M.; Batasheva, S.; Stavitskaya, A.; Glotov, A.; Vinokurov, V. Interfacial Self-Assembly in Halloysite Nanotube Composites. *Langmuir* **2019**, *35*, 8646–8657. [[CrossRef](#)]
32. Massaro, M.; Noto, R.; Riela, S. Past, Present and Future Perspectives on Halloysite Clay Minerals. *Molecules* **2020**, *25*, 4863. [[CrossRef](#)]
33. Massaro, M.; Casiello, M.; D'Accolti, L.; Lazzara, G.; Nacci, A.; Nicotra, G.; Noto, R.; Pettignano, A.; Spinella, C.; Riela, S. One-pot synthesis of ZnO nanoparticles supported on halloysite nanotubes for catalytic applications. *Appl. Clay Sci.* **2020**, *189*, 105527. [[CrossRef](#)]
34. Massaro, M.; Colletti, C.G.; Lazzara, G.; Milioto, S.; Noto, R.; Riela, S. Halloysite nanotubes as support for metal-based catalysts. *J. Mater. Chem. A* **2017**, *5*, 13276–13293. [[CrossRef](#)]
35. Abdullayev, E.; Joshi, A.; Wei, W.; Zhao, Y.; Lvov, Y. Enlargement of halloysite clay nanotube lumen by selective etching of aluminum oxide. *ACS Nano* **2012**, *6*, 7216–7226. [[CrossRef](#)]
36. Choi, S.; Chaudhari, S.; Shin, H.; Cho, K.; Lee, D.; Shon, M.; Nam, S.; Park, Y. Polydopamine-modified halloysite nanotube-incorporated polyvinyl alcohol membrane for pervaporation of water-isopropanol mixture. *J. Ind. Eng. Chem.* **2022**, *105*, 158–170. [[CrossRef](#)]
37. Mazurova, K.; Glotov, A.; Kotelev, M.; Eliseev, O.; Gushchin, P.; Rubtsova, M.; Vutolkina, A.; Kazantsev, R.; Vinokurov, V.; Stavitskaya, A. Natural aluminosilicate nanotubes loaded with RuCo as nanoreactors for Fischer-Tropsch synthesis. *Sci. Technol. Adv. Mater.* **2022**, *23*, 17–30. [[CrossRef](#)]
38. Lisuzzo, L.; Cavallaro, G.; Milioto, S.; Lazzara, G. Halloysite nanotubes filled with salicylic acid and sodium diclofenac: Effects of vacuum pumping on loading and release properties. *J. Nanostruct. Chem.* **2021**, *11*, 663–673. [[CrossRef](#)]
39. Dasireddy, V.D.B.C.; Likoza, B. The role of copper oxidation state in Cu/ZnO/Al₂O₃ catalysts in CO₂ hydrogenation and methanol productivity. *Renew. Energy* **2019**, *140*, 452–460. [[CrossRef](#)]
40. Talam, S.; Karumuri, S.R.; Gunnam, N. Synthesis, Characterization, and Spectroscopic Properties of ZnO Nanoparticles. *ISRN Nanotechnol.* **2012**, *2012*, 372505. [[CrossRef](#)]
41. Muniz, F.T.; Miranda, M.A.; Morilla Dos Santos, C.; Sasaki, J.M. The Scherrer equation and the dynamical theory of X-ray diffraction. *Acta Cryst. A Found Adv.* **2016**, *72*, 385–390. [[CrossRef](#)] [[PubMed](#)]
42. Duma, Z.G.; Moma, J.; Langmi, H.W.; Louis, B.; Parkhomenko, K.; Musyoka, N.M. Towards High CO₂ Conversions Using Cu/Zn Catalysts Supported on Aluminum Fumarate Metal-Organic Framework for Methanol Synthesis. *Catalysts* **2022**, *12*, 1104. [[CrossRef](#)]
43. Pike, S.D.; García-Trenco, A.; White, E.R.; Leung, A.H.; Weiner, J.; Shaffer, M.S.; Williams, C.K. Colloidal Cu/ZnO catalysts for the hydrogenation of carbon dioxide to methanol: Investigating catalyst preparation and ligand effects. *Catal. Sci. Technol.* **2017**, *7*, 3842–3850. [[CrossRef](#)]
44. Şeker, B.; Dizaji, A.K.; Balci, V.; Uzun, A. MCM-41-supported tungstophosphoric acid as an acid function for dimethyl ether synthesis from CO₂ hydrogenation. *Renew. Energy* **2021**, *171*, 47–57. [[CrossRef](#)]

45. Alharbi, W.; Kozhevnikova, E.F.; Kozhevnikov, I.V. Dehydration of Methanol to Dimethyl Ether over Heteropoly Acid Catalysts: The Relationship between Reaction Rate and Catalyst Acid Strength. *ACS Catal.* **2015**, *5*, 7186–7193. [[CrossRef](#)]
46. Sobczak, J.; Wysocka, I.; Murgrabia, S.; Rogala, A. A Review on Deactivation and Regeneration of Catalysts for Dimethyl Ether Synthesis. *Energies* **2022**, *15*, 5420. [[CrossRef](#)]
47. Yu, Y.; Sun, D.; Wang, S.; Xiao, M.; Sun, L.; Meng, Y. Heteropolyacid Salt Catalysts for Methanol Conversion to Hydrocarbons and Dimethyl Ether: Effect of Reaction Temperature. *Catalysts* **2019**, *9*, 320. [[CrossRef](#)]
48. Legagneux, N.; Basset, J.M.; Thomas, A.; Lefebvre, F.; Goguet, A.; Sa, J.; Hardacre, C. Characterization of silica-supported dodecatungstic heteropolyacids as a function of their dehydroxylation temperature. *Dalton. Trans.* **2009**, 2235–2240. [[CrossRef](#)]
49. Pechenkin, A.; Potemkin, D.; Rubtsova, M.; Snytnikov, P.; Plyusnin, P.; Glotov, A. CuO-In₂O₃ Catalysts Supported on Halloysite Nanotubes for CO₂ Hydrogenation to Dimethyl Ether. *Catalysts* **2021**, *11*, 1151. [[CrossRef](#)]
50. Choi, E.; Song, K.; An, S.; Lee, K.; Youn, M.; Park, K.; Jeong, S.; Kim, H. Cu/ZnO/AlOOH catalyst for methanol synthesis through CO₂ hydrogenation. *Korean J. Chem. Eng.* **2017**, *35*, 73–81. [[CrossRef](#)]
51. Kang, S.-H.; Bae, J.W.; Prasad, P.S.S.; Oh, J.-H.; Jun, K.-W.; Song, S.-L.; Min, K.-S. Influence of Ga addition on the methanol synthesis activity of Cu/ZnO catalyst in the presence and absence of alumina. *J. Ind. Eng. Chem.* **2009**, *15*, 665–669. [[CrossRef](#)]
52. Mao, D.; Yang, W.; Xia, J.; Zhang, B.; Song, Q.; Chen, Q. Highly effective hybrid catalyst for the direct synthesis of dimethyl ether from syngas with magnesium oxide-modified HZSM-5 as a dehydration component. *J. Catal.* **2005**, *230*, 140–149. [[CrossRef](#)]
53. Din, I.U.; Shaharun, M.S.; Alotaibi, M.A.; Alharthi, A.I.; Naeem, A. Recent developments on heterogeneous catalytic CO₂ reduction to methanol. *J. CO₂ Util.* **2019**, *34*, 20–33. [[CrossRef](#)]
54. Lombi, E.; Scheckel, K.G.; Kempson, I.M. In situ analysis of metal (loid) s in plants: State of the art and artefacts. *Environ. Exp. Bot.* **2011**, *72*, 3–17. [[CrossRef](#)]
55. Zhang, T.; Bui, J.C.; Li, Z.; Bell, A.T.; Weber, A.Z.; Wu, J. Highly selective and productive reduction of carbon dioxide to multicarbon products via in situ CO management using segmented tandem electrodes. *Nat. Catal.* **2022**, *5*, 202–211. [[CrossRef](#)]
56. Oleinick, A.; Sliusarenko, O.; Svir, I.; Amatore, C. Review—Nanostructured Electrodes as Random Arrays of Active Sites: Modeling and Theoretical Characterization. *J. Electrochem. Soc.* **2019**, *167*, 013530. [[CrossRef](#)]
57. Singh, R.; Tripathi, K.; Pant, K.K.; Parikh, J.K. Unravelling synergetic interaction over tandem Cu-ZnO-ZrO₂/hierarchical ZSM5 catalyst for CO₂ hydrogenation to methanol and DME. *Fuel* **2022**, *318*, 123641. [[CrossRef](#)]
58. Arena, F.; Italiano, G.; Barbera, K.; Bordiga, S.; Bonura, G.; Spadaro, L.; Frusteri, F. Solid-state interactions, adsorption sites and functionality of Cu-ZnO/ZrO₂ catalysts in the CO₂ hydrogenation to CH₃OH. *Appl. Catal. A Gen.* **2008**, *350*, 16–23. [[CrossRef](#)]
59. Bonura, G.; Migliori, M.; Frusteri, L.; Cannilla, C.; Catizzone, E.; Giordano, G.; Frusteri, F. Acidity control of zeolite functionality on activity and stability of hybrid catalysts during DME production via CO₂ hydrogenation. *J. CO₂ Util.* **2018**, *24*, 398–406. [[CrossRef](#)]
60. Etim, U.J.; Zhang, C.; Zhong, Z. Impacts of the Catalyst Structures on CO₂ Activation on Catalyst Surfaces. *Nanomaterials* **2021**, *11*, 3265. [[CrossRef](#)]
61. Xin, C.; Hu, M.; Wang, K.; Wang, X. Significant Enhancement of Photocatalytic Reduction of CO₂ with H₂O over ZnO by the Formation of Basic Zinc Carbonate. *Langmuir* **2017**, *33*, 6667–6676. [[CrossRef](#)] [[PubMed](#)]
62. Shi, G.; Chen, Q.; Zhang, Q.; Cai, W.; Li, Z.; Zhai, S.; Yu, H.; Tan, F.; Wang, Y. Morphology effect of ZnO support on the performance of Cu toward methanol production from CO₂ hydrogenation. *J. Saudi Chem. Soc.* **2020**, *24*, 42–51. [[CrossRef](#)]
63. Weatherbee, G.D.; Bartholomew, C.H. Hydrogenation of CO₂ on group VIII metals: IV. Specific activities and selectivities of silica-supported Co, Fe, and Ru. *J. Catal.* **1984**, *87*, 352–362. [[CrossRef](#)]
64. Kattel, S.; Yan, B.; Yang, Y.; Chen, J.G.; Liu, P. Optimizing binding energies of key intermediates for CO₂ hydrogenation to methanol over oxide-supported copper. *J. Am. Chem. Soc.* **2016**, *138*, 12440–12450. [[CrossRef](#)]
65. Etim, U.J.; Song, Y.; Zhong, Z. Improving the Cu/ZnO-Based Catalysts for Carbon Dioxide Hydrogenation to Methanol, and the Use of Methanol As a Renewable Energy Storage Media. *Front. Energy Res.* **2020**, *8*, 545431. [[CrossRef](#)]
66. Al-Faze, R.; Finch, A.; Kozhevnikova, E.F.; Kozhevnikov, I.V. Dehydration of methanol and ethanol over silica-supported heteropoly acids in the gas phase: Surface-type versus bulk-type catalysis mechanism. *Appl. Catal. A Gen.* **2020**, *597*, 117549. [[CrossRef](#)]
67. Enferadi-Kerenkan, A.; Do, T.O.; Kaliaguine, S. Heterogeneous catalysis by tungsten-based heteropoly compounds. *Catal. Sci. Technol.* **2018**, *8*, 2257–2284. [[CrossRef](#)]
68. Tao, M.; Xue, L.; Sun, Z.; Wang, S.; Wang, X.; Shi, J. Tailoring the Synergistic Bronsted-Lewis acidic effects in Heteropolyacid catalysts: Applied in Esterification and Transesterification Reactions. *Sci. Rep.* **2015**, *5*, 13764. [[CrossRef](#)]
69. Ateka, A.; Pérez-Uriarte, P.; Sánchez-Contador, M.; Ereña, J.; Aguayo, A.T.; Bilbao, J. Direct synthesis of dimethyl ether from syngas on CuO ZnO MnO/SAPO-18 bifunctional catalyst. *Int. J. Hydrogen Energy* **2016**, *41*, 18015–18026. [[CrossRef](#)]
70. Dai, B.; Cao, S.; Xie, H.; Zhou, G.; Chen, S. Reduction of CO₂ to CO via reverse water-gas shift reaction over CeO₂ catalyst. *Korean J. Chem. Eng.* **2017**, *35*, 421–427. [[CrossRef](#)]

Disclaimer/Publisher’s Note: The statements, opinions and data contained in all publications are solely those of the individual author(s) and contributor(s) and not of MDPI and/or the editor(s). MDPI and/or the editor(s) disclaim responsibility for any injury to people or property resulting from any ideas, methods, instructions or products referred to in the content.